*Proc. Natl. Acad. Sci. USA*
Vol. 91, pp. 1741–1745, March 1994
Biophysics

# Segmental dynamics of the cytoplasmic domain of erythrocyte band 3 determined by time-resolved fluorescence anisotropy: Sensitivity to pH and ligand binding

BERNARD J.-M. THEVENIN*†, N. PERIASAMY‡, STEPHEN B. SHOHET*, AND A. S. VERKMAN‡

Departments of *Laboratory Medicine and ‡Medicine and Physiology, University of California, San Francisco, CA 94143-0134

*Communicated by Daniel Branton, September 24, 1993*

ABSTRACT **Interactions between the erythrocyte membrane and its skeleton are mediated primarily by binding of cytoskeletal components to a conformationally sensitive structure, the cytoplasmic domain of band 3 (cdb3). To examine the nanosecond segmental motions of cdb3, band 3 was labeled selectively by fluorescein maleimide at Cys-201 near the proposed hinge in cdb3 about which pH-dependent conformational changes occur. Time-resolved anisotropy of labeled cdb3 in isolated form and in stripped erythrocyte membranes was measured by parallel-acquisition frequency-domain microfluorimetry. Samples had a single-component fluorescein lifetime of ≈4 ns. Multifrequency phase and modulation data (5–200 MHz) fitted well to a segmental motion model containing two correlation times ($\tau_{1c}$ and $\tau_{2c}$) and two limiting anisotropies ($r_{1\infty}$ and $r_{2\infty}$). Measurements in protease-cleaved and denatured samples indicated that $\tau_{1c}$ (100–150 ps) corresponded to rapid rotation of bound fluorescein and $\tau_{2c}$ (2–5 ns) corresponded to segmental motion of cdb3. Both motions were hindered as quantified by nonzero $r_{1\infty}$ and $r_{2\infty}$. The strong pH dependence of segmental motion correlated with that of cdb3 conformation measured by intrinsic tryptophan fluorescence. Significant changes in cdb3 segmental motion occurred upon interactions with the small ligands 2,3-bisphosphoglycerate and calcium and several glycolytic enzymes known to bind to the N terminus of band 3. These time-resolved fluorescence measurements of the nanosecond segmental dynamics of a labeled membrane protein provide evidence for the sensitivity of cdb3 conformation to ligand binding and suggest long-range structural communication through cdb3.**

The best known function of band 3, the major integral protein of erythrocyte membranes, is the electroneutral exchange of anions across the plasma membrane (1). However, band 3 has several additional functions, many of which are mediated by interaction of its cytoplasmic domain with various soluble factors and enzymes (2). For example, the association between the cytoplasmic domain of band 3 (cdb3) and ankyrin provides the primary attachment site for the spectrin-based membrane skeleton (3, 4). Other components that interact with cdb3 include band 4.1, band 4.2, hemoglobin, and several glycolytic enzymes (2–4). To accommodate the binding of multiple substrates, cdb3 has an extended asymmetric structure (2). Whereas the binding sites for hemoglobin and glycolytic enzymes are restricted to the extreme N terminus of cdb3 (2), ankyrin and band 4.1 appear to interact also with distal regions of cdb3 (5–7). Several experiments suggest the existence of a flexible "hinge" near the middle of cdb3 (2, 8); the hinge may permit flexion of cdb3 to facilitate ligand binding to noncontiguous band 3 sequences.

There is increasing evidence that band 3 has a dynamic structure. Band 3 appears to exist *in situ* as an equilibrium mixture of dimers and tetramers held together by noncovalent interactions (1, 9). In addition, cdb3 is thought to be poised in a facile equilibrium among three native conformations differing by their degree of bending at the hinge (2). These conformations are sensitive to protonation–deprotonation reactions and differ substantially—the Stokes' radius of cdb3 increases from 55 to 66 Å between pH 6.5 and 10 (8). Finally, several recent observations suggest structural communication between distant regions of band 3, such as between the N terminus and the intramembrane anion channel or the cytoplasmic cysteine cluster located on the C-terminal segment of cdb3 (10–13). The multiple static and dynamic conformations of band 3 are likely to have functional importance. For example, the three pH-dependent conformations of cdb3 have widely different affinities for ankyrin and may regulate the interaction between the membrane cytoskeleton and the bilayer (14, 15); also, a conserved region of flexibility between cdb3 and the membrane-spanning domain, which is missing in hereditary ovalocytosis, appears to be critical for maintenance of normal erythrocyte shape and deformability (16, 17). Despite extensive functional and molecular studies on band 3, there is little information about the (time-dependent) dynamic motions of band 3. Although the global rotation of fluorescently labeled band 3 in the plane of the erythrocyte membrane has been measured (18, 19), to our knowledge, nothing is known about the segmental motions of subdomains of band 3.

The purpose of this study was to characterize the nanosecond dynamics of cdb3 by time-resolved anisotropy measurements of a fluorescein reporter at Cys-201 in the vicinity of the proposed hinge. The ability to label selectively cdb3 in isolated form and *in situ* and recent advances in parallel-acquisition frequency-domain microfluorimetry (20) made possible the analysis of time-resolved anisotropy in terms of rapid picosecond rotation of fluorescein at its labeling site and slower nanosecond segmental motion of cdb3. We find (*i*) extensive pH-dependent conformational changes in cdb3 that are consistent with bending at the hinge, (*ii*) conformational sensitivity of cdb3 upon interaction with small ligands and glycolytic enzymes, and (*iii*) considerable flexibility of the proximal subdomain of cdb3 located near the membrane. In addition, these studies provide an approach to measure the coupled nanosecond segmental dynamics of a labeled protein and subnanosecond rotation of the attached fluorophore.

## MATERIALS AND METHODS

**Preparation of KI-Extracted Inside-Out Vesicles (KI-IOVs) and cdb3.** KI-IOVs were prepared from fresh blood as described (14, 21) except that 0.025% Tween 20 was included

The publication costs of this article were defrayed in part by page charge payment. This article must therefore be hereby marked "*advertisement*" in accordance with 18 U.S.C. §1734 solely to indicate this fact.

Abbreviations: cdb3, cytoplasmic domain of band 3; KI-IOV, KI-extracted inside-out vesicle; CA, carbonic anhydrase; FM-KI-IOVs, FM-cdb3, and FM-CA, fluorescein maleimide-labeled KI-IOVs, cdb3, and CA, respectively.

†To whom reprint requests should be addressed.

in the 1 M KI buffer to maximize band 4.2 stripping. cdb3 was released from stripped IOVs in 15% (vol/vol) MeOH with chymotrypsin (1.75 μg/ml) at −9°C and isolated as reported (22).

**Labeling of the Cys Cluster in Isolated cdb3 and in KI-IOVs.** KI-IOVs (1.5 mg/ml) and cdb3 (1 mg/ml) were incubated with fluorescein maleimide (FM; 70 and 100 mM, respectively) at pH 7 for 1 h at 0°C, quenched with dithiothreitol, and dialyzed extensively. Labeling stoichiometries were measured by absorbance at pH 8 in 0.2% SDS, by using $\varepsilon$ = 78,000 $M^{-1}\cdot cm^{-1}$ for conjugated fluorescein at 492 nm, 43 kDa for cdb3, 30 kDa for carbonic anhydrase (CA), and a band 3 protein fraction of 55% in KI-IOVs. Labeling stoichiometries were 1.07 and 0.25 for fluorescein maleimide-labeled cdb3 (FM-cdb3) and CA (FM-CA), respectively; for KI-IOVs, >60% of total labeling was on band 3. Labeling of cdb3 and KI-IOVs was cooperative up to a stoichiometry of 1 (anticooperative above 1); similar time-resolved data were obtained with labeling stoichiometries of 0.5–1.1.

**Fluorescence Measurements.** Time-resolved fluorescence was measured by parallel-acquisition frequency-domain microfluorimetry using components of a multiharmonic Fourier-transform SLM 48000 (Urbana, IL) fluorimeter (23). Differential phase angles and modulation ratios were obtained in parallel at 40 discrete modulation frequencies between 5 and 200 MHz. Samples (0.15 mm thick) were sandwiched between two cover glasses and positioned on the stage of an inverted epifluorescence microscope. Fluorescence was excited with polarized impulse-modulated light from an Ar laser (488 nm). Time-resolved fluorescence and anisotropy were determined as described (23). Differential phase angles and modulation ratios were fitted to models of anisotropy decay by standard nonlinear regression procedures (24). These included a single hindered rotator model, $r(t) = r_0[(1 - r_\infty/r_0)e^{-t/\tau_c} + (r_\infty/r_0)]$, where $r(t)$ is the time-resolved anisotropy, $r_0$ is the maximum anisotropy, $\tau_c$ is the rotational correlation time, and $r_\infty$ is the residual anisotropy at infinite time; a two-component anisotropy decay model, $r(t) = r_0[f_1e^{-t/\tau_{1c}} + f_2e^{-t/\tau_{2c}}]$, where $\tau_{1c}$ and $\tau_{2c}$ are the rotational correlation times of the two components with fractional amplitudes $f_1$ and $f_2$; and a two-component segmental motion model:

$$r(t) = r_0\{[(1 - r_{1\infty}/r_0)e^{-t/\tau_{1c}} + (r_{1\infty}/r_0)] \\ [(1 - r_{2\infty}/r_0)e^{-t/\tau_{2c}} + (r_{2\infty}/r_0)]\}, \quad [1]$$

where $r_{1\infty}$ and $r_{2\infty}$ are "residual anisotropies" at infinite time associated with each rotator, and $\tau_{1c}$ and $\tau_{2c}$ are the corresponding rotational correlation times. This final model is the product of two coupled hindered rotations (see *Discussion*).

## RESULTS

**Specific Labeling of the Cytoplasmic Cys Cluster of Band 3 with Fluorescein.** Fig. 1 *A* and *B* shows the labeling specificity for the two principal preparations used, cdb3 and KI-IOVs, respectively. Band 3 was stoichiometrically labeled with FM under conditions that label Cys-201, the most reactive of the two clustered cysteines of cdb3 (25). Fig. 1*A* also shows that of the two major tryptic fragments of cdb3 (referred to as N-terminal 21-kDa and C-terminal 20-kDa subdomains, ref. 2), only the faster migrating 20-kDa fragment containing the Cys cluster was labeled. Under similar labeling conditions in KI-IOVs, band 3 was predominantly labeled (Fig. 1*B*, lanes 7 and 9). Tryptic cleavage released only a single labeled fragment corresponding to the 20-kDa subdomain (lanes 8 and 10), consistent with selective labeling of cdb3 Cys cluster in KI-IOVs. Conjugation of fluorescein reduced the electrophoretic mobility of cdb3 and its 20-kDa fragment. Mobility was reduced further by a second label (data not shown); this property confirmed that each cdb3 was labeled with only one fluorescein.

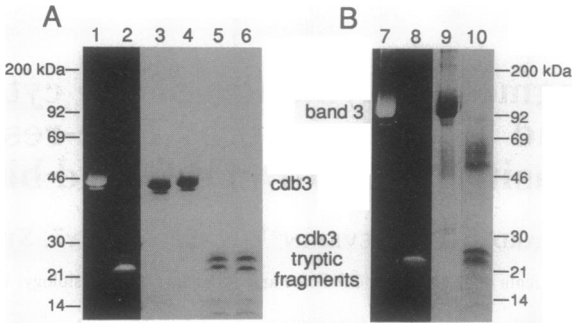


FIG. 1. Labeling of the band 3 cytoplasmic Cys cluster in isolated cdb3 (*A*) and in KI-IOVs (*B*). Fluorescence is shown in lanes 1, 2, 7, and 8. Coomassie staining is in lanes 3–6, 9, and 10. (*A*) Lanes: 1 and 4, FM-cdb3; 2 and 5, trypsin-cleaved FM-cdb3; 3, unlabeled cdb3; 6, unlabeled trypsin-cleaved cdb3. (*B*) Lanes: 7 and 9, FM-KI-IOVs; 8 and 10, trypsin-cleaved FM-KI-IOVs. FM-cdb3 and cdb3 (each at 0.25 mg/ml) and KI-IOVs (0.5 mg/ml) were incubated with trypsin (50 and 5 μg/ml, respectively) at pH 8 for 30 min at 0°C to cleave cdb3 into its N-terminal 21-kDa and C-terminal 20-kDa subdomains, which have anomalously slow electrophoretic mobilities. The faint labeling above the 20-kDa labeled fragment is not from the 21-kDa fragment, but rather a (minor) larger C-terminal fragment.

**Time-Resolved Fluorescence Measurements of Fluorescein-Labeled Band 3.** Initial measurements of steady-state fluorescence anisotropy of FM-cdb3 revealed a strong decrease between pH 6 and 10 with a marked transition around pH 8.6 (data not shown). Intrinsic FM-cdb3 tryptophan fluorescence, a reporter of cdb3 conformation (8), was also found to increase maximally around pH 8.6. This suggested that the motions of the bound fluorescein were sensitive to cdb3 conformation and that the dynamics of fluorescein motions could be exploited as conformational reporter. To resolve the steady-state anisotropy of FM-cdb3 into individual parameters describing fluorescein rotations, time-resolved measurements were carried out by parallel-acquisition frequency-domain microfluorimetry.

Fig. 2*A* shows representative multifrequency phase and modulation data for the lifetime of FM-cdb3. The data fitted well to a single-component lifetime of 4.25 ns, independent of pH and other experimental maneuvers (see below). The lifetime of FM-CA was 4.0 ns and was also pH-independent. For FM-labeled KI-IOVs (FM-KI-IOVs), the data fitted best to a two-component lifetime decay containing a major component at 3.8–4.0 ns and a minor component at 0.8–1.4 ns (<15% fractional amplitude); the short lifetime may be due to nonspecific fluorescein binding and was ignored for analysis of time-resolved anisotropy data.

Representative multifrequency phase and modulation data obtained for time-resolved fluorescence anisotropy measurements of FM-cdb3 are also shown in Fig. 2. Fig. 2 *B–D* shows data obtained at pH 7.5, 6.4, and 9.2, respectively. The original phase and modulation values are remarkably pH-dependent. Quantitative analysis of phase and modulation data requires fitting to a suitable model for anisotropy decay. For fluorescein bound to the Cys cluster, the data did not fit adequately to a single-correlation time-hindered rotator model or a two-correlation time model (Fig. 2*B*). However, the data were fitted satisfactorily to a four-parameter model describing segmental motion (Eq. 1). The shorter correlation time $\tau_{1c}$ (100–150 ps) described the rapid motion of the fluorescein molecule in its hindered environment; the longer correlation time $\tau_{2c}$ (2–5 ns) was attributed to the segmental motion of the protein segment bearing the probe. All data

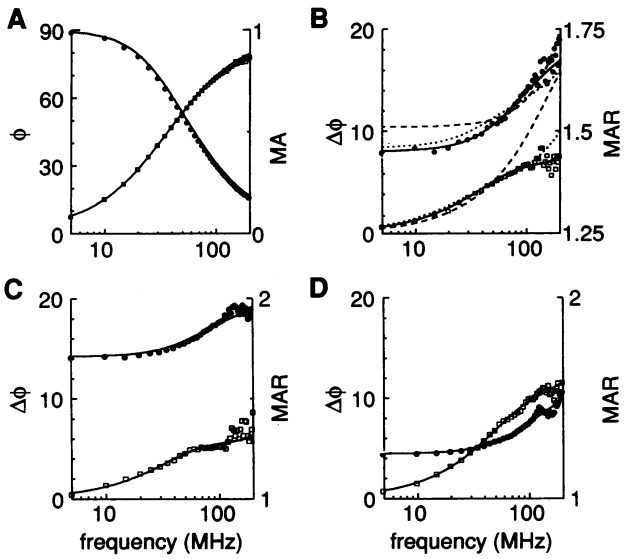


FIG. 2. Phase angles ($\phi$ and $\Delta\phi$, solid circles) and modulation amplitude ratios (MA and MAR, open squares) obtained with FM-cdb3. Representative data for the measurement of the fluorescence lifetime at pH 8 (*A*) and time-resolved anisotropy at pH 7.5 (*B*), 6.5 (*C*), and 9.2 (*D*). Buffers were as in Fig. 3. Solid lines represent a fit of the data to a single lifetime of 4.25 ns (*A*) or to the segmental motion model, Eq. 1 (*B–D*). The dashed, dotted, and solid lines in *B* show data fit to a single hindered rotator model ($\chi^2$ = 103), a two-component isotropic rotator model ($\chi^2$ = 4.3), and a segmental motion model, Eq. 1 ($\chi^2$ = 0.81), respectively.

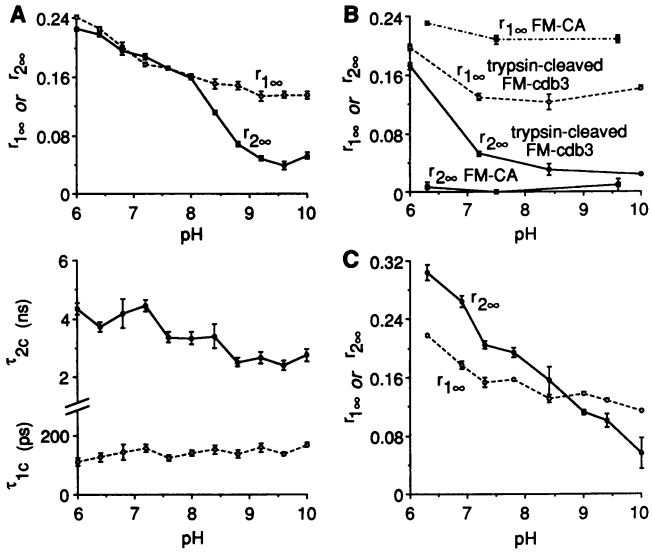


FIG. 3. pH dependence of the segmental motion parameters obtained for FM-cdb3 (*A*), trypsin-cleaved FM-cdb3 (*B*) and FM-CA (*B*), and FM-KI-IOVs (*C*). Error bars in Figs. 3–5 are SEMs. Buffers: 40 mM $Na_2HPO_4$/40 mM $NaH_2BO_3$, titrated to the indicated pH. Tryptic cleavage at the hinge was as in Fig. 4. Mean correlation times were $\tau_{1c}$ = 130 ps and $\tau_{2c}$ = 2.3 ns for trypsin-cleaved FM-cdb3 and $\tau_{1c}$ = 110 ps and $\tau_{2c}$ = 11.0 ns for FM-CA. The apparent biphasic character of the pH dependence of $r_{2\infty}$ in *C* was retained whether the data were analyzed with floating or fixed ($\tau_{1c}$ = 150 ps and $\tau_{2c}$ = 4.1 ns) correlation times. The value of $\tau_{2c}$ (11 ns) for FM-CA corresponds to rotation of the whole enzyme (26).

below were analyzed according to the segmental motion model.

**pH Dependence of the Time-Resolved Anisotropy of Fluorescein Bound to the Cys Cluster of Band 3.** Analysis of the time-resolved fluorescence anisotropy of FM-cdb3 revealed strong pH sensitivity for both $r_{1\infty}$ and $r_{2\infty}$ (Fig. 3*A Upper*). A moderate increase in $r_{1\infty}$ occurred mainly below pH 7.2, whereas a large decrease in $r_{2\infty}$ occurred between pH 8.0 and 9.2. The correlation time $\tau_{2c}$ corresponding to segmental motion also decreased between pH 8.0 and 9.2 (Fig. 3*A Lower*); $\tau_{1c}$ was pH-insensitive. The results suggested that the fall in FM-cdb3 steady-state anisotropy between pH 7.5 and 9.5 was primarily due to the increase in segmental motion centered at pH ≈8.6 where FM-cdb3 changes conformation.

To test whether changes in segmental motion were indeed related to changes in cdb3 conformation, measurements were undertaken after limited tryptic digestion to cleave cdb3 at its hinge. The anisotropy parameters were pH-insensitive above pH 7.2 (Fig. 3*B*), and $r_{2\infty}$ and $\tau_{2c}$ were similar to that for uncleaved FM-cdb3 at pH >9.5. This result implied that changes in the segmental motion of FM-cdb3 above pH 7.5 were attributable to conformational bending of cdb3 about its hinge and that the restriction to segmental motion was relieved at high pH. To assess the specificity of the pH dependence of $r_{1\infty}$ and $r_{2\infty}$, measurements were carried out on a control protein FM-CA, which had virtually pH-insensitive rotational parameters (Fig. 3*B*).

Similar experiments were conducted with FM-KI-IOVs. As for FM-cdb3, $r_{1\infty}$ and $r_{2\infty}$ were strongly pH-dependent (Fig. 3*C*). Fast and slow correlation times were found to be pH insensitive ($\tau_{1c}$ ≈ 150 ps and $\tau_{2c}$ ≈ 4.1 ns). Although the pH dependence of $r_{1\infty}$ was similar to that measured for FM-cdb3, $r_{2\infty}$ decreased strongly with increasing pH below pH 7.2. The decrease in $r_{2\infty}$ between pH 7.8 and 10, though less pronounced than that for FM-cdb3, probably corresponds to a cytoplasmic conformational change in band 3; trypsin cleavage of cdb3 in KI-IOVs also reduced $r_{2\infty}$ at pH 7.5 to the level obtained at high pH with uncleaved FM-KI-IOVs (see below). These results are in qualitative agreement with those obtained for isolated cdb3 despite imperfect labeling selectivity in FM-KI-IOVs.

To further investigate the dependence of the fitted parameters on protein structure, measurements were conducted at pH 7.5 after urea denaturation and extensive proteolytic digestion (Fig. 4); both maneuvers eliminated the restriction on segmental motion ($r_{2\infty}$ ≈ 0) for FM-cdb3 and FM-KI-IOVs. Most of the restriction was also lost upon cdb3 cleavage at the hinge. In contrast, $r_{1\infty}$ was relatively insensitive to these maneuvers. These results support the conclu-

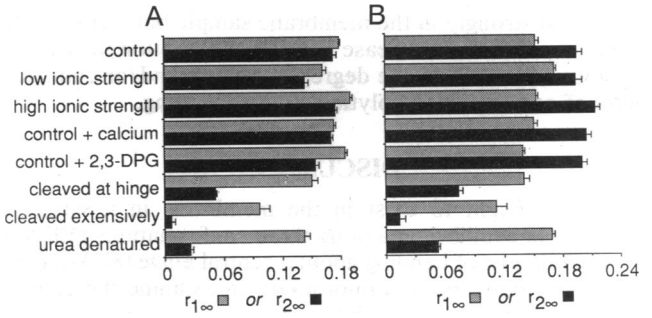


FIG. 4. Sensitivity of $r_{1\infty}$ (shaded bars) and $r_{2\infty}$ (solid bars) to ionic strength, small ligands, and other conditions for FM-cdb3 (*A*) and FM-KI-IOVs (*B*) at pH 7.5. Buffers: 67 mM $Na_2HPO_4$ (control), 1 mM $Na_2HPO_4$ (low ionic strength), control + 1 M KCl, control + 1 mM calcium, and control + 20 mM 2,3-bisphosphoglycerate (2,3-DPG). FM-cdb3 and FM-KI-IOVs (≈1.5 mg/ml) were selectively cleaved at the hinge with trypsin (50 μg/ml) for 30 min at 0°C and extensively digested with trypsin, chymotrypsin, and papain (each at 100 μg/ml) for 1 h at 25°C. Denaturation was in 8 M urea. All $\tau_{1c}$ values were not significantly different from controls (≈130 ps). For FM-cdb3 and FM-KI-IOVs, $\tau_{2c}$ values differing significantly from controls (3.5 and 4.1 ns) were 2.3 and 2.5 ns (cleaved at hinge), 0.6 and 1.2 ns (cleaved extensively), and 2.1 and 2.1 ns (urea denatured), respectively.

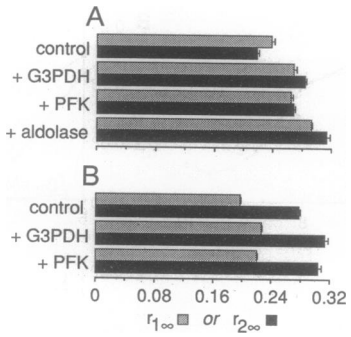


FIG. 5. Effect of glycolytic enzyme binding on the segmental motion parameters obtained for FM-cdb3 (*A*) and FM-KI-IOVs (*B*). Shaded and solid bars represent $r_{1\infty}$ and $r_{2\infty}$, respectively. Control buffer was 10 mM $NaH_2PO_4$ (pH 6.5). FM-cdb3 (1.1 mg/ml) and FM-KI-IOVs (1.4 mg/ml) were incubated with stoichiometric excesses of glyceraldehyde-3-phosphate dehydrogenase (G3PDH; ≈5×), phosphofructose kinase (PFK; ≈1×), or aldolase (≈10×) for >2 h before measurements. $\tau_{1c}$ values for all samples were not significantly different from controls (≈110 ps). For FM-cdb3, $\tau_{2c}$ values were 4.7 ns (control), 4.4 ns (+ G3PDH), 5.6 ns (+ PFK), and 5.9 ns (+aldolase). For FM-KI-IOVs, $\tau_{2c}$ values were 4.7 ns (control), 11.1 ns (+G3PDH), and 8.9 ns (+PFK).

sion that the probe is sensitive to conformational changes related to the bending of cdb3 about its hinge.

**Conformational Sensitivity of cdb3 to Small Ligands and Glycolytic Enzymes.** For FM-cdb3 at pH 7.5, there were small but significant effects of ionic strength and binding of 2,3-bisphosphoglycerate and calcium on $r_{1\infty}$ and/or $r_{2\infty}$ (Fig. 4*A*). These were not caused by small variations in the fitted correlation times because analyses carried out with fixed (mean) correlation times ($\tau_{1c}$ = 130 ps and $\tau_{2c}$ = 3.6 ns) yielded similar differences. Experiments were also conducted with FM-KI-IOVs to determine whether this apparent conformational sensitivity of cdb3 occurred in native membranes. Ionic strength and small ligands also affected $r_{1\infty}$ and/or $r_{2\infty}$ significantly (Fig. 4*B*), albeit differently than with FM-cdb3, possibly because of the anchorage of cdb3 to the membrane *in situ*.

At relatively low pH and ionic strength, glycolytic enzymes bind the N terminus of band 3 (2) causing a large increase in $r_{1\infty}$ and $r_{2\infty}$ for both FM-cdb3 (Fig. 5*A*) and FM-KI-IOVs (Fig. 5*B*). Whereas $\tau_{1c}$ did not change with enzyme binding, $\tau_{2c}$ increased strongly in the membrane sample but weakly with isolated cdb3. The decrease in segmental motion indicates a profound increase in the degree of rigidity and/or compactness of cdb3 upon glycolytic enzymes binding.

## DISCUSSION

cdb3 is thought to exist in the membrane in a sensitive metastable equilibrium among three conformations differing by their degree of bending about a central hinge (8). We used frequency-domain microfluorimetry to examine the conformational sensitivity of cdb3 in isolated form and *in situ* in erythrocyte membranes. cdb3 was labeled with fluorescein at the Cys cluster, which is near the hinge, so that probe rotation should be sensitive to bending, a contention supported by the correlation between pH-dependent changes in intrinsic tryptophan fluorescence and steady-state fluorescence anisotropy. Analysis of the time-resolved anisotropy indeed revealed pH-dependent changes paralleling changes in cdb3 conformation (Fig. 3). The sensitivity of fluorescein motions to cdb3 conformation was then utilized to examine the effect of pH and various factors that associate with or affect cdb3 structure (Figs. 4 and 5).

Analysis of time-resolved anisotropy of labeled cdb3 (both isolated and *in situ*) required two correlation times and an anisotropy decay model describing segmental motion (Eq. **1**). The shorter (100–150 ps) and longer (2–5 ns) correlation times corresponded to hindered rotations of bound fluorescein and segmental motions of the labeled polypeptide segment, respectively; models of similar complexity incorporating unhindered rotation(s) were not adequate (Fig. 2). The anisotropy decay model used here is an extension of previous models of segmental mobility of a fluorophore linked to a rigid biopolymer (27, 28) and provided an adequate fit to the data with the fewest parameters. In addition, the fitted parameters provided physical insight into cdb3 motions and changed predictably in a variety of maneuvers including proteolysis and denaturation.

The faster correlation time $\tau_{1c}$ was attributed to the rapid diffusion of fluorescein in its binding pocket. $\tau_{1c}$ was similiar to that of (free) fluorescein in aqueous solutions (≈100 ps) and was relatively insensitive to pH and other maneuvers. For all conditions studied, the nonzero value of $r_{1\infty}$ indicated geometrically restricted motion. If the restricted motion is assumed to occur in a cone with hard walls (29), then the "cone angle" for rotation (wobbling) of the probe was never greater than 52° even after proteolysis or denaturation. This restriction was also observed with FM-CA (Fig. 3*B*) and other labeled proteins (data not shown). Thus, attachment to a polypeptide substantially limits probe motion, and additional restriction beyond this threshold is imposed by geometrical constraints from the protein at the labeling site.

The slower correlation time $\tau_{2c}$ was attributed to segmental motion of the band 3 polypeptide that was also hindered as described by $r_{2\infty}$. $r_{2\infty}$ and $\tau_{2c}$ values strongly decreased with proteolysis and denaturation as predicted (Fig. 4). The value of $\tau_{2c}$ (≈4 ns) suggests that the effective size of the wobbling labeled segment is substantially smaller than cdb3 or even its 20-kDa C-terminal subdomain. Indeed, a 4-ns correlation time corresponds to a nonhydrated spherical particle of ≈13 kDa and both hydration and asymmetry would further decrease this size by 1.4- to 2.4-fold (26, 28). Also, $\tau_{2c}$ decreased 1.5- to 2-fold when the labeled segment was cleaved at one node of flexibility (the hinge, Figs. 3 and 4), as theoretically predicted (30). Hence, the C-terminal subdomain of cdb3 is highly flexible because of multiple partially flexible sequences or a single major node of flexibility located within ≈7 kDa of the hinge. It is noteworthy that the C-terminal subdomain contains two sequences with the same proline content as the hinge—residues 259–274 (6.7 kDa from the hinge) and 322–337—which by Chou–Fasman analysis (31) can form β-turns (data not shown); a high propensity for β-turns for the 35 residues next to the hinge is also predicted. The similar $\tau_{2c}$ value for isolated and membrane-associated cdb3 also suggests considerable flexibility of the region between the labeling site and the membrane.

The restriction to segmental motion of cdb3 was strongly pH-dependent (Fig. 3). Motion was least hindered above pH 9.6 when cdb3 structure is least compact ($r_{2\infty} \approx 0.04$ corresponds to a 64° cone angle) and highly restricted below pH 6.8 when cdb3 structure is most compact ($r_{2\infty} \approx 0.22$ corresponds to a 35° cone angle). This restriction was dramatically reduced when cdb3 was cleaved at the hinge, denatured, or proteolyzed extensively. Similar observations were made for band 3 *in situ*, although the restriction to segmental motion was higher. Although flexible, the region between the hinge and the membrane domain may limit the torsional motion of the labeled segment. The diagram in Fig. 6 shows a working model for cdb3 dynamic structure. cdb3 is represented as an elongated structure with a central hinge controlling the degree of flexion of its two subdomains. The C-terminal subdomain is shown to contain several β-turns proposed to account for its observed high flexibility.

The significant effects of ionic strength and binding of small ligands (2,3-bisphosphoglycerate and calcium) on $r_{1\infty}$ and $r_{2\infty}$

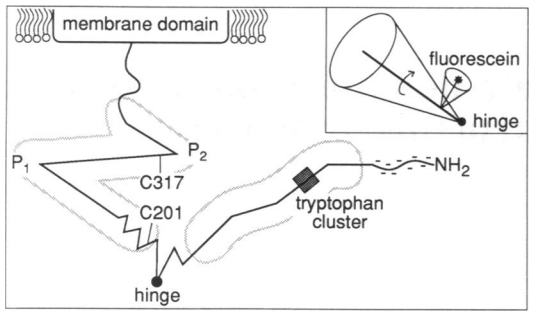


FIG. 6. Proposed model of cdb3 dynamic structure showing an asymmetric structure for cdb3 with a highly flexible central hinge (residues 175–190) about which pH-dependent conformational changes take place and a flexible region connecting cdb3 to the membrane domain. The C-terminal segment contains several β-turns proposed to account for the flexibility of cdb3 C-terminal of Cys-201, the labeling site (see text). Cys-201 and -317 are close together as reported (25), and their distance to the Trp cluster in the N-terminal domain varies with the pH-dependent conformation (8).

(Fig. 4) suggest that band 3 structure is sensitive to environment and binding events. Although ionic strength effects could involve spatial changes near the labeling site, that of small ligands are probably mediated by a global conformational change in cdb3. Indeed, association with 2,3-bisphosphoglycerate destabilizes cdb3 structure (32) and calcium binds the distal anionic N-terminal segment of band 3 (33, 34). Glycolytic enzymes and hemoglobin also bind electrostatically to the unstructured N terminus of band 3, with no evidence for an interaction near the hinge. Based on the structural communication between the hemoglobin binding site and cdb3 Cys cluster (13), we believe that the strong dependence of fluorescein rotation on glycolytic enzyme binding (Fig. 5) results from a change in cdb3 conformation. The substantial increases in $r_{1\infty}$ and $r_{2\infty}$ suggest that cdb3 becomes considerably more compact, possibly by additional bending at the hinge, similar to that seen at very low pH. The additional bending would bring the glycolytic enzyme-associated N terminus closer or in contact with the membrane domain and could account for the decrease in flexibility of the C-terminal subdomain observed with labeled band 3 but not isolated cdb3. In conclusion, the significant rigidification of cdb3 upon association with glycolytic enzymes as well as the structural effect of 2,3-bisphosphoglycerate and calcium binding constitute evidence for long-range structural communication through cdb3.

We thank Drs. S. E. Bicknese and J. R. Abney for helpful discussions, Dr. A. Van Hoek for the Chou–Fasman analysis of cdb3, and D. B. Zimet for computational assistance. This work was supported by National Institutes of Health Grants DK16095 and DK43840 and by a W. Duncan MacMillan Trust grant-in-aid. This is publication 127 from the MacMillan–Cargill Hematology Research Laboratory.

1. Jennings, M. L. (1989) *Annu. Rev. Biophys. Chem.* **18,** 397–430.
2. Low, P. S. (1986) *Biochim. Biophys. Acta* **864,** 145–167.
3. Bennett, V. (1985) *Annu. Rev. Biochem.* **54,** 273–304.
4. Goodman, S. R., Krebs, K. E., Whitfield, C. F., Riederer, B. M. & Zagon, I. S. (1988) *CRC Crit. Rev. Biochem.* **23,** 171–234.
5. Willardson, B. M., Thevenin, B. J.-M., Harrison, M. L., Kuster, W. M., Benson, M. D. & Low, P. S. (1989) *J. Biol. Chem.* **264,** 15893–15899.
6. Davis, L., Lux, S. E. & Bennett, V. (1989) *J. Biol. Chem.* **264,** 9665–9672.
7. Lombardo, C. R., Willardson, B. M. & Low, P. S. (1992) *J. Biol. Chem.* **267,** 9540–9546.
8. Low, P. S., Westfall, M. A., Allen, D. P. & Appell, K. C. (1984) *J. Biol. Chem.* **259,** 13070–13076.
9. Casey, J. R. & Reithmeier, A. F. (1991) *J. Biol. Chem.* **266,** 15726–15737.
10. Salhany, J. M., Cordes, K. A. & Gaines, E. D. (1980) *Biochemistry* **19,** 1447–1454.
11. Bursaux, E., Hilly, M., Bluze, A. & Poyart, C. (1984) *Biochim. Biophys. Acta* **777,** 253–260.
12. Ducis, J., Kandrach, A. & Racker, E. (1988) *J. Biol. Chem.* **263,** 8544–8550.
13. Salhany, J. M. & Cassoly, R. (1989) *J. Biol. Chem.* **264,** 1399–1404.
14. Thevenin, B. J.-M. & Low, P. S. (1990) *J. Biol. Chem.* **265,** 16166–16172.
15. Low, P. S., Willardson, B. M., Mohandas, N., Rossi, M. & Shohet, S. B. (1984) *Blood* **77,** 1581–1586.
16. Mohandas, N., Winardi, R., Knowles, D., Leung, A., Parra, M., George, E., Conboy, J. & Chasis, J. (1992) *J. Clin. Invest.* **89,** 686–692.
17. Schofield, A. E., Tanner, M. J. A., Pinder, J. C., Clough, B., Bayley, P. M., Nash, G. B., Dluzewski, A. R., Reardon, D. M., Cox, T. M., Wilson, R. J. M. & Gratzer, W. B. (1992) *J. Mol. Biol.* **223,** 949–958.
18. Matayoshi, E. D. & Jovin, T. M. (1991) *Biochemistry* **30,** 3527–3538.
19. McPherson, R. A., Sawyer, W. H. & Tilley, L. (1992) *Biochemistry* **31,** 512–518.
20. Fushimi, K. & Verkman, A. S. (1991) *J. Cell Biol.* **112,** 719–725.
21. Bennett, V. (1983) *Methods Enzymol.* **96,** 313–325.
22. Appell, K. C. & Low, P. S. (1981) *J. Biol. Chem.* **256,** 11104–11111.
23. Verkman, A. S., Armijo, M. & Fushimi, K. (1991) *Biophys. Chem.* **40,** 117–125.
24. Calafut, T. M., Dix, J. A. & Verkman, A. S. (1989) *Biochemistry* **28,** 5051–5058.
25. Thevenin, B. J.-M., Willardson, B. M. & Low, P. S. (1989) *J. Biol. Chem.* **264,** 15886–15892.
26. Yguerabide, J., Epstein, H. F. & Stryer, L. (1970) *J. Mol. Biol.* **51,** 573–590.
27. Lipari, G. & Szabo, A. (1980) *Biophys. J.* **30,** 489–506.
28. Bucci, E. & Steiner, R. F. (1991) *Biophys. Chem.* **30,** 199–224.
29. Kinosita, K., Jr., Kawato, S. & Ikegami, A. (1977) *Biophys. J.* **20,** 289–305.
30. Wegener, W. A., Dowben, R. M. & Koester, V. J. (1980) *J. Chem. Phys.* **73,** 4086–4097.
31. Chou, P. Y. & Fasman, G. D. (1989) *Biochemistry* **13,** 211–222.
32. Moriyama, R., Lombardo, C. R., Workman, R. F. & Low, P. S. (1993) *J. Biol. Chem.* **268,** 10990–10996.
33. Charuk, J. H. M., Pirraglia, C. A. & Reithmeier, R. A. F. (1990) *Anal. Biochem.* **188,** 123–131.
34. Salhany, J. M. & Cordes, K. A. (1991) *Biochem. Biophys. Res. Commun.* **174,** 975–982.